Centrum voor Wiskunde en Informatica

REPORT*RAPPORT*

The Interface between Fresh and Salt Groundwater in Heterogeneous Aquifers: A Numerical Approach

J.F. Scheid, R.J. Schotting

Modelling, Analysis and Simulation (MAS)

MAS-R9735 December 31, 1997

Report MAS-R9735
ISSN 1386-3703

CWI
P.O. Box 94079
1090 GB Amsterdam
The Netherlands

The Interface between Fresh and Salt Groundwater in Heterogeneous Aquifers: A Numerical Approach

J.F. Scheid
Université de Paris-Sud
Laboratoire d'Analyse numérique d'Orsay, Paris-Sud, 91405 Orsay, France
email: Jean-Francois.Scheid@math.u-psud.fr

R.J. Schotting[1]
CWI
P.O. Box 94079, 1090 GB Amsterdam, The Netherlands
email: ruuds@cwi.nl

ABSTRACT
In this paper we study the behavior of a sharp interface between fresh and salt groundwater, in horizontally extended heterogeneous aquifers. The heterogeneities considered are discontinuities in intrinsic permeability. Each fluid has a constant, but different specific weight, while the viscosities are equal. The difference in specific weight induces fluid movement, which in turn causes motion of the interface. We are especially interested in the behavior of interfaces crossing discontinuities in permeability.
The governing equations are an elliptic equation for the stream function, coupled with an interface motion equation for the time evolution of the interface. A finite element method is used to solve the equation for the stream function and a front tracking scheme to compute the time evolution of the (discrete) interface movement.
We compare numerical results with some (semi-)analytical results of simplified interface problems in both homogeneous and heterogeneous aquifers. Some attention is given to hydrodynamically instable situations, i.e. when a heavier fluid is on top of a lighter fluid.

1991 Mathematics Subject Classification: 73V05, 76S05, 82B24
Keywords and Phrases: Fresh/salt interface model, Groundwater, FEM, Similarity solutions, Stability, Gravity driven flow, Heterogeneities
Note: Work carried out under project MAS1.3 "Partial Differential Equations in Porous Media Research".

1 Introduction

Gravity induces a flow in a porous medium if horizontal density gradients are present. These horizontal gradients produce vorticity, which in turn causes (density-driven) fluid flow. This insight is mainly due to the work of Wooding [21], [22] and Elder [8].

Fresh and salt groundwater are essentially miscible fluids. When brought in contact in a porous medium, a mixing zone will develop, which is caused by molecular diffusion and hydrodynamical dispersion. The latter is additional mixing due to local velocity variations which are caused by local variations in permeability. In most practical situations the width of the transition zone is small compared to the extensions of the aquifer. This motivates to assume the existence of an interface between the fluids: the specific weight changes abruptly from one value to an other value. Thus in this approximation we treat the strictly miscible fluids as immiscible. In their mathematical formulation, interface models lead to so called free boundary problems.

The implications of the existence of an interface between fresh and salt groundwater have been studied by De Josselin De Jong [12]. In that case, the horizontal density gradients across the interface are singular and the interface becomes a surface source (in three space dimensions) or a line source (in a vertical cross section) of vorticity. The flow of the separate fluids is rotation free, while the rotation of the total flow is produced by

the (singular) vorticity distribution along the interface. As a consequence, the velocity component normal to the interface is continuous and the velocity component tangential to the interface exhibits a discontinuity across the interface: the shear flow.

In a later paper, De Josselin De Jong [11], derived a nonlinear diffusion-type equation to approximate density-driven flow in a vertical cross section of horizontally extended aquifers confined by two impermeable layers. The derivation is based on the Dupuit assumption, i.e. the horizontal component of the specific discharge is constant in each fluid and jumps at the interface. The advantage of this approach is that the two-dimensional flow problem reduces to a one-dimensional initial value problem in terms of the interface height. Solutions of this approximate equation give insight in the time evolution and flow properties of the full problem, in particular with respect to the large time behavior, i.e. for relatively flat interfaces.

Following the original work of De Josselin De Jong [12], Chan Hong et.al. [6] studied the movement of the interface between fresh and salt groundwater by numerical means. They formulate the problem in terms of an elliptic (Poisson) equation for the stream function describing the flow and a hyperbolic equation for the time evolution of the interface. The parameterization of the interface is of the form $z = u(x,t)$, where respectively x and z denote the horizontal and vertical coordinate of a point located at the interface. The elliptic problem is solved using a finite element method (moving mesh) while the interface motion equation is solved explicitly in time, by means of a predictor-corrector method. Chan Hong et. al. [6] compare numerical results with solutions of simplified problems, based on the Dupuit approximation with respect to the horizontal flow. Only homogeneous flow domains are considered.

We focus on the transient behavior of an interface in heterogeneous aquifers, including those cases where it is not possible to parameterize the interface according to $z = u(x,t)$ or $x = u(z,t)$. We modified the existing finite element code [6] to allow for heterogeneous intrinsic permeability distributions in the flow domain and developed a front tracking method, to compute the discrete time evolution of the interface. The latter is inspired by ideas developed in Dupaix et. al. [7] and Scheid [18]. Points along the discretized interface are displaced by computing an approximate normal direction and an approximate normal velocity from the stream function along the interface.

The heterogeneities considered are discontinuities in intrinsic permeability. In case of a vertical discontinuity in permeability, i.e. two adjacent regions with different piecewise constant permeability, we solve a related Dupuit problem in terms of a similarity solution. It turns out that the numerical solution converges towards a similarity solution as $t \to \infty$.

In case of two horizontal layers with different piecewise constant permeability, i.e a horizontal discontinuity, it is not possible to obtain a semi-explicit solution of a related Dupuit problem. Therefore it is difficult to validate the numerical solutions, even when the mass balance is conserved up to a small error. Moreover, if the initial interface is vertical, a hydrodynamically unstable zone will develop in the vicinity of the discontinuity in permeability, where the heavy fluid (salt ground water) is on top of the lighter one (fresh groundwater). Rayleigh-Taylor instabilities (fresh-salt fingers) are observed in the computational results, as soon as salt water is on top of fresh water.

A normal-mode linear stability analysis shows that instabilities (fresh-salt fingers) of any wave length λ (or wave number ω) can occur in the fingering pattern. List [14], studied the stability of the uniform horizontal motion of two miscible fluids of different density in a saturated, homogeneous porous medium, both theoretically (by means of a normal-mode linear stability analysis) and experimentally. List showed the existence of a critical wave length λ_0. Perturbations with wave length $\lambda < \lambda_0$ decay in time, while perturbations with $\lambda > \lambda_0$ grow. The number λ_0 is related to the dispersion coefficient D. In the limit $D \to 0$, i.e. in case of a fresh-salt interface, we obtain $\lambda_0 = 0$, implying that perturbations of any wave length will grow in time.

However, in the results of the interface computations we observe that only instabilities of a certain minimum wave length or finger width grow in time. The latter is determined by the coarseness of the (piecewise linear) discretization of the interface.

In addition, we consider a problem in a homogeneous flow domain. Van Duijn & Philip [17] studied bounds on the behavior of slumping brine mounds. Two modifications of the approximate Dupuit interface motion equation, see De Josselin De Jong [11], are applied to the slumping of finite two-dimensional brine mounds. Both modifications lead to simple similarity solutions. One gives upper bounds on the time-scales of the process and the other lower bounds. We check the validity of these approximate bounds against a numerical solution of the full problem. The results are in excellent agreement with the predictions in [17].

The organization is as follows. In Section 2 we give the governing flow equations and give the boundary and initial conditions. A description of the numerical procedure is given in Section 3. In Section 4 we compare computed results with two approximate problems in a homogeneous flow domain, that are based on the Dupuit assumption. The first problem concerns the time evolution of a rotation linear interface. We compare the results obtained with the front tracking scheme, with the predictor-corrector scheme (as proposed in [6]) and with the corresponding Dupuit approximation. This problem is included mainly to gain confidence in the front tracking method. The second homogeneous problem concerns the slumping of brine mounds. We verify numerically the bounds on the time scale of the slumping process of decaying brine mounds [17]. In Section 5 a general expression is derived for the shape of the interface in an infinitesimal small neighborhood of a discontinuity in intrinsic permeability. This expression is used for verification of the numerical results. The special case of a vertical discontinuity in permeability is considered in Section 6. We derive an approximate Dupuit similarity solution and compare it with the large time behavior of numerical solutions of the full problem. A horizontal discontinuity in permeability is considered in Section 7. Special attention is given to the growth of Rayleigh-Taylor instabilities that occur in the vicinity of the discontinuity in permeability. Section 8 contains the conclusions and some discussion.

2 The model

The governing equations are the continuity equation for incompressible fluids and Darcy's law, i.e. the momentum balance equation. These equations can be combined into a single Poison equation for the stream function, which describes the flow induced by the difference in specific weight of the fluids. From the solution of the stream function equation, i.e. for a given specific weight distribution at a certain time level, we determine the normal component of the velocity at the interface. The result is used to displace the interface in time.

2.1 The stream function equation

We consider flow of an incompressible fluid of variable specific weight γ and constant viscosity μ, in a rectangular domain with variable intrinsic permeability κ. The flow domain is given by the strip $\Omega = I \times (0, h)$, where I denotes the interval $(-R, R)$ with $R > 0$, such that $R >> h$ $(h > 0)$. The strip represents a vertical cross section of a horizontally extended aquifer, bounded from above and below by impermeable layers.

Let $\mathbf{q}$ denote the specific discharge vector, p the fluid pressure and $\mathbf{e}_z$ the unit vector pointing in the positive (upward) z-direction. The fluid movement is governed by Darcy's law, i.e.

$$\frac{\mu}{\kappa}\mathbf{q} + \nabla p + \gamma \mathbf{e}_z = 0 \qquad \text{in } \Omega \tag{2.1}$$

and the continuity equation given by

$$\text{div } \mathbf{q} = 0 \qquad \text{in } \Omega. \tag{2.2}$$

The latter expresses expresses the incompressibility of the fluid. At the boundary $\partial\Omega$ we assume a no-flow condition, i.e.

$$\mathbf{q} \cdot \mathbf{n} = 0 \qquad \text{on } \partial\Omega, \tag{2.3}$$

where $\mathbf{n}$ denotes the outward normal unit vector on $\partial\Omega$. By taking the two-dimensional curl of equation (2.1), we obtain

$$\text{curl } \left(\frac{\mu}{\kappa}\mathbf{q}\right) + \text{curl } (\gamma \mathbf{e}_z) = 0 \qquad \text{in } \Omega. \tag{2.4}$$

Here the curl of a vector function $\mathbf{a} = (a_x, a_z)$ must be understood in the sense that $\text{curl } \mathbf{a} := \partial a_x/\partial z - \partial a_z/\partial x$. Since the flow satisfies equation (2.2) we can introduce a stream function ψ such that

$$\mathbf{q} = \text{curl } \psi = \left(-\frac{\partial \psi}{\partial z}, \frac{\partial \psi}{\partial x}\right). \tag{2.5}$$

Substitution this expression in (2.4) yields

$$\text{div } \left(\frac{\mu}{\kappa}\nabla\psi\right) = -\frac{\partial \gamma}{\partial x} \qquad \text{in } \Omega. \tag{2.6}$$

This equation has to be interpreted in the weak sense, see Van Duijn & De Josselin De Jong [9] for details. The no-flow condition (2.3) implies that ψ is constant at $\partial\Omega$. The value of ψ on $\partial\Omega$ can be chosen arbitrarily. For convenience we set:

$$\psi = 0 \qquad \text{on } \partial\Omega. \tag{2.7}$$

Next, we introduce the interface approximation: the interface $\Gamma(t)$ separates fresh groundwater, with specific weight γ_f, and salt groundwater, with specific weight γ_s, where $0 < \gamma_f < \gamma_s$. This implies that γ is discontinuous at the interface and thereby the right-hand side of 2.6 a singularity. Consequences of the latter are summarized in Section 2.2. Thus, given an interface at a certain time $t \geq 0$, the solution of (2.6) subject to (2.7), determines the stream function distribution in flow domain Ω, and by (2.5) the corresponding discharge $\mathbf{q}$.

The heterogeneities considered in this paper are discontinuities in intrinsic permeability. We confine ourselves to the special case of piecewise constant permeability distributions: a vertical heterogeneity given by

$$\kappa = (\kappa_2 - \kappa_1)H(x) + \kappa_1 \ \text{ for } \ x \in I, \tag{2.8}$$

and a horizontal heterogeneity given by

$$\kappa = (\kappa_1 - \kappa_2)H(z - h/2) + \kappa_2 \ \text{ for } \ z \in [0, h], \tag{2.9}$$

where H denotes the Heaviside function: $H(\xi) = 1$ for $\xi > 0$ and $H(\xi) = 0$ for $\xi < 0$.

2.2 Properties of the stream function

Properties of the of the stream function, and thereby the induced discharge field, can be derived from problem (2.6)-(2.7), see e.g. [9], [6], [11]. In particular, we are interested in conditions on the stream function and the corresponding discharges at the interface and at discontinuities in permeability. Combining these conditions enables us to derive a fundamental expression for the behavior of an interface crossing a discontinuity in permeability, see Section 5.

Without loss of generality, we assume that the interface can be parameterized according to $z = u(x,t)$ in a small neighborhood of the discontinuity in permeability. Then the fluid domain Ω can be decomposed in 4 regions $\Omega_{i,j}$ for $i = 1, 2$ and $j = f, s$. Here $\Omega_{i,f}$ (respectively $\Omega_{i,s}$) denotes the domain occupied by fresh water (respectively salt water) in the region where $\kappa(x,z) = \kappa_i$, for $i = 1, 2$. Let Γ_i denote the part of the interface Γ in the region where $\kappa(x,z) = \kappa_i$ for $i = 1, 2$ and let Σ_j denote the boundary between the region where $\kappa = \kappa_1$ and that of $\kappa = \kappa_2$ in the part of the domain where $\gamma = \gamma_j$ for $j = f, s$, see Figure 1 for the case of a horizontal heterogeneity. Then let $\mathbf{n}$ (respectively $\mathbf{s}$) denote the outward normal unit vector (respectively the tangential unit vector) to the boundary $\partial\Omega_{i,j}$ of $\Omega_{i,j}$.

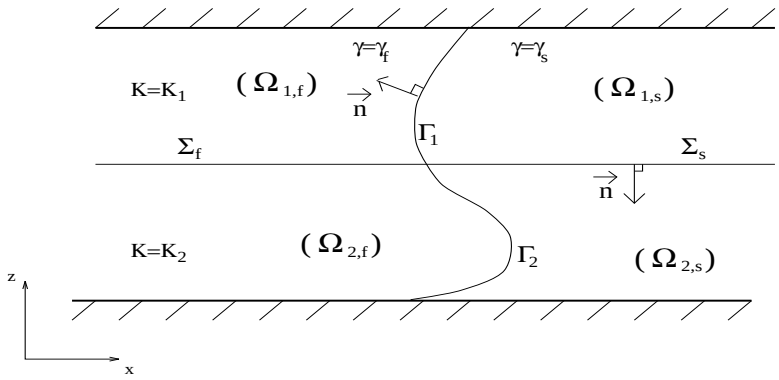

Figure 1
The case of a horizontal heterogeneity. Definition of the domains.

In case of sufficiently smooth interface $\Gamma(t)$, problem (2.6)-(2.7) in terms of ψ, can be written as a set problems on the subdomains $\Omega_{i,j}$ for $i = 1, 2$ and $j = f, s$, with conditions at the interface. It can be shown that a solution $\psi(x, z, t)$ of (2.6)-(2.7) satisfies the following basic properties: for $i = 1, 2$ and $j = f, s$ we have

$$
\begin{array}{lll}
(a) & -\Delta\psi_{i,j} = 0 & \text{in } \Omega_{i,j} \\
\left.\begin{array}{ll} (b) & \psi_{i,f} = \psi_{i,s} \\ (c) & \dfrac{\partial\psi_{i,f}}{\partial n} - \dfrac{\partial\psi_{i,s}}{\partial n} = -\dfrac{\kappa_i}{\mu}\left(\gamma_s - \gamma_f\right) n_x \end{array}\right\} & & \text{on } \Gamma_i \\
\left.\begin{array}{ll} (d) & \psi_{1,j} = \psi_{2,j} \\ (e) & \kappa_2 \dfrac{\partial\psi_{1,j}}{\partial n} - \kappa_1 \dfrac{\partial\psi_{2,j}}{\partial n} = 0 \end{array}\right\} & & \text{on } \Sigma_j \\
(f) & \psi = 0 & \text{on } \partial\Omega_{i,j}
\end{array}
\tag{2.10}
$$

Here n_x denotes the x-component of the unit vector normal to the interface. Conditions (b) and (d) express the continuity of the stream function at Γ_i and Σ_j, implying $\partial\psi_{i,f}/\partial s = \partial\psi_{i,s}/\partial s$ for $i = 1, 2$, i.e. continuity of the discharge component normal to Γ_i, and $\partial\psi_{1,j}/\partial s = \partial\psi_{2,j}/\partial s$ for $j = f, s$, i.e. continuity of the discharge component normal to Σ_j. Expression (c) is the shear flow along the interface: the discharge tangential to the interface in discontinuous when crossing the interface. The discharge tangential to the discontinuity in permeability also exhibits a jump and satisfies (g). De Josselin De Jong [11]) arrived at the same result for the homogeneous case using physical arguments.

2.3 Time evolution of the interface

In order to allow for more general interface shapes, we do not parameterize the interface explicitly, as in e.g. Chan Hong et. al. [6] or [11]. Given a solution $\psi = \psi(x, z, t)$ of problem (2.6)-(2.7), the normal component of the velocity at the interface $\Gamma(t)$ satisfies

$$
V_n = \frac{1}{\varepsilon}\mathbf{q}\cdot\mathbf{n} = \frac{1}{\varepsilon}\text{curl }\psi\cdot\mathbf{n} \qquad \text{at} \quad \Gamma(t), \tag{2.11}
$$

where $\mathbf{n}$ denotes the normal unit vector at $\Gamma(t)$, pointing into the fresh water region and ε the porosity of the porous medium. The latter is assumed to be constant. Evaluation of (2.11) yields

$$
V_n = \frac{1}{\varepsilon}\frac{\partial\psi}{\partial s} \qquad \text{at} \quad \Gamma(t), \tag{2.12}
$$

where $\partial/\partial s$ denotes the tangential direction along the interface.

Remark:

When the interface shape allows parametrization of the form $z = u(x, t)$ in Ω, the interface motion equation can be written as

$$
\frac{\partial u}{\partial t} = \frac{1}{\varepsilon}\frac{\partial}{\partial x}\left\{\psi\left(x, u(x,t), t\right)\right\} \qquad \text{in } I \times \mathbb{R}^+. \tag{2.13}
$$

This particular form is due to Chan Hong et. al. [6]. Suppose that an interface touches the domain boundaries at $z = 0$ and $z = h$. Let the corresponding x-coordinates be given by $S_1(t)$ (toe) and $S_2(t)$ (top). It was also shown in [6] that $S_1(t)$ and $S_2(t)$ satisfy the differential equations

$$
\dot{S}_1(t) = -\frac{1}{\varepsilon}\lim_{x\to S_1(t)}\frac{\psi\left(x, u(x,t), t\right)}{u(x,t)} \quad \text{and} \quad \dot{S}_2(t) = \frac{1}{\varepsilon}\lim_{x\to S_2(t)}\frac{\psi\left(x, u(x,t), t\right)}{h - u(x,t)}. \tag{2.14}
$$

We use these expressions to compute the velocity of the top and toe under the assumption that the interface can be parameterized in a small neighborhood of the lower and upper domain boundaries.

The variables are redefined according to

$$x := \frac{x}{h}, \quad z := \frac{z}{h}, \quad \kappa := \frac{\kappa}{\kappa_0} \quad t := t\frac{(\gamma_s - \gamma_f)\kappa_0}{\varepsilon \mu h}, \tag{2.15}$$

and

$$\psi := \psi \frac{\mu}{(\gamma_s - \gamma_f)\kappa_0 h}, \quad \Gamma := \frac{\Gamma}{h}, \tag{2.16}$$

where κ_0 denotes a reference permeability. Then equations (2.6) and (2.11), subject to boundary and initial conditions, lead to the problem of finding the stream function $\psi = \psi(x, z, t)$ and $\Gamma(t)$ satisfying:

$$(P) \begin{cases} -\text{div}\left(\frac{1}{\kappa}\nabla\psi\right) = \frac{\partial}{\partial x}\left(\gamma(x,z,t)\right) & \text{in } \Omega \times \mathbb{R}^+, \\ \psi = 0 & \text{on } \partial\Omega \times \mathbb{R}^+, \\ V_n = \frac{\partial \psi}{\partial s} & \text{on } \Gamma(t),\ t \in \mathbb{R}^+, \\ \Gamma(t=0) = \Gamma_0. \end{cases} \tag{2.17}$$

In dimensionless form, the equations for the velocities of the top and toe of the interface, are given by

$$\dot{S}_1(t) = -\lim_{x \to S_1(t)} \frac{\psi\left(x, u(x,t), t\right)}{u(x,t)} \quad \text{and} \quad \dot{S}_2(t) = \lim_{x \to S_2(t)} \frac{\psi\left(x, u(x,t), t\right)}{1 - u(x,t)}, \tag{2.18}$$

where we redefined u according to $u := u/h$.

3 The numerical method

In this section we give a numerical algorithm for solving Problem (P). The procedure consists of three steps. We first solve the elliptic problem for the stream function, for a given interface Γ at time level t, see also [6]. Next, we compute an approximation of the normal component of the velocity at the interface. Finally we apply a discrete front tracking method to obtain an approximation of the position of the interface at the new time level.

3.1 Discretization of the stream function equation

Let $\gamma^k(x,z)$ and Γ^k be respectively the specific weight and the interface at time t^k. The stream function ψ is determined by the solution of problem

$$(P_\psi^k) \begin{cases} -\text{div}\left(\frac{1}{\kappa}\nabla\psi\right) = \frac{\partial}{\partial x}\left(\gamma^k(x,z)\right), & \text{for } (x,z) \in \Omega, \\ \psi = 0, & \text{on } \partial\Omega. \end{cases} \tag{3.1}$$

We solve (P_ψ^k) using a finite element method. The weak formulation of (P_ψ^k) is obtained by multiplying equation (3.1) by a test function $v \in H_0^1(\Omega)$ and integration by parts:

$$\int_\Omega \frac{1}{\kappa}\nabla\psi.\nabla v = \int_\Omega \gamma^k(x,z)\frac{\partial v}{\partial x}, \quad \text{for all } v \in H_0^1(\Omega). \tag{3.2}$$

We decompose domain Ω at time t^k into two subdomains Ω_f^k and Ω_s^k, being respectively the subdomain of fresh water and salt water. Moreover, we assume that the interface Γ^k between Ω_f^k and Ω_s^k is smooth enough. After integration by parts of the right-hand side of (3.2) we obtain the following weak formulation of Problem (P_ψ^k)

Find $\psi \in H_0^1(\Omega)$ such that

$$\int_\Omega \frac{1}{\kappa} \nabla\psi.\nabla v = (\gamma_f - \gamma_s) \int_{\Gamma^k} v\ n_x\ d\sigma, \quad \text{for all } v \in H_0^1(\Omega), \tag{3.3}$$

where n_x denotes the x-component of the unit vector normal to the interface Γ^k, pointing into Ω_f^k.

Let $\mathcal{T}_h$ be a triangularization of $\overline{\Omega}$. If we apply the finite element method with piecewise linear basis functions, then the discretized problem is given by:

Find $\psi_h \in V_h$ such that

$$\int_\Omega \frac{1}{\kappa} \nabla\psi_h \cdot \nabla v_h = (\gamma_f - \gamma_s) \int_{\Gamma_h^k} v_h\ n_{h,x}\ d\sigma, \quad \text{for all } v \in V_h, \tag{3.4}$$

where $V_h = \left\{ v_h \in C(\overline{\Omega}) \mid \forall\, T \in \mathcal{T}_h,\ v_h \text{ is linear on } T \text{ and } v_h = 0 \text{ on } T \right\}$. Here, Γ_h^k is a piecewise linear approximation of Γ^k, while n_h denotes an approximation of the unit vector normal to Γ^k.

Let $(\phi_i)_{i=1,\ldots,N}$ be the piecewise linear basis function of V_h. We decompose ψ_h on this basis, i.e.

$$\psi_h(x,z) = \sum_{i=1}^{N} \psi_i \phi_i(x,z) \ \text{ for } \ (x,z) \in \Omega. \tag{3.5}$$

Then Problem (3.4) is equivalent to

$$\sum_{i=1}^{N} \psi_i \int_\Omega \frac{1}{\kappa} \nabla\phi_i.\nabla\phi_j = (\gamma_f - \gamma_s) \int_{\Gamma_h^k} \phi_j n_{h,x} d\sigma, \quad \text{for all } j = 1, \ldots, N. \tag{3.6}$$

Following [6], we apply a moving mesh method which enables to generate a new triangularization of Ω at each time step. Let $\Omega_{h,f}^k$ denote the fresh water domain and $\Omega_{h,s}^k$ the salt water domain. These domains are separated by the piecewise linear approximation of interface Γ_h^k. The triangularization of $\Omega_{h,f}^k$ and $\Omega_{h,s}^k$ is respectively $\tau_{h,f}^k$ and $\tau_{h,s}^k$. These are constructed such that Γ_h^k always coincides with sides of triangles of $\tau_{h,f}^k$ and $\tau_{h,s}^k$. We refine the mesh in the neighborhood of Γ_h^k. The meshes are generated, using the mesh generator of the SEPRAN finite element package, which is developed at Delft University of Technology.

3.2 Discretization of the interface motion: front tracking

Let ψ^k be the stream function at time level $t^k = k\Delta t$, where Δt denotes the time step and $k = 0, 1, ..K$. Then the normal component of the velocity of a point at the interface is given by

$$V_n^k = \frac{\partial \psi^k}{\partial s^k} = \nabla\psi^k \cdot \mathbf{s}^k$$

where $\mathbf{s}^k$ denotes the unit vector tangential to Γ^k. Since $V_n^k = \frac{\partial \Gamma}{\partial t}(k\Delta t) \cdot \mathbf{n}(k\Delta t)$, we compute the interface position at time level $t^{k+1} = (k+1)\Delta t$ explicitly in time using

$$\Gamma^{k+1} \cdot \mathbf{n}(k\Delta t) = \Gamma^k \cdot \mathbf{n}(k\Delta t) + \Delta t\ V_n.$$

Let Γ_h^k be defined by a set of nodal points $(P_i^k)_{i=1,\ldots,I}$, hence

$$\Gamma_h^k = \left\{ \left[P_i^k P_{i+1}^k \right], i = 1, \ldots, I-1,\ P_1^k \text{ and } P_I^k \in \partial\Omega \right\}.$$

The displacement of each nodal point is given by

$$\overrightarrow{P_i^k P_i^{k+1}} = \Delta t\ V_{n,i}^k \approx \Delta t\ D_i^k \cdot \mathbf{s}_i^k, \quad \text{for } i = 2, \ldots, I-1$$

where $V_{n,i}^k$ denotes the approximation of $V_n(P_i^k)$ and D_i^k the approximation of $\nabla\psi^k(P_i^k)$. The unit vector at point P_i^k given by by the approximation

$$\mathbf{s}_i^k = \frac{\overrightarrow{P_{i-1}^k P_{i+1}^k}}{\| \overrightarrow{P_{i-1}^k P_{i+1}^k} \|}. \tag{3.7}$$

Since

$$\psi^k(P_{i-1}^k) \approx \psi^k(P_i^k) + \overrightarrow{P_i^k P_{i-1}^k} \cdot \nabla\psi^k(P_i^k) \;\text{ and }\; \psi^k(P_{i+1}^k) \approx \psi^k(P_i^k) + \overrightarrow{P_i^k P_{i+1}^k} \cdot \nabla\psi^k(P_i^k) \tag{3.8}$$

we have

$$\frac{\overrightarrow{P_{i-1}^k P_{i+1}^k}}{\| \overrightarrow{P_{i-1}^k P_{i+1}^k} \|} . \nabla\psi^k(P_i^k) \simeq \frac{\psi^k(P_{i+1}^k) - \psi^k(P_{i-1}^k)}{\| \overrightarrow{P_{i-1}^k P_{i+1}^k} \|}.$$

This motivates to choose

$$V_{n,i}^k = D_i^k \cdot \mathbf{s}_i^k = \frac{\psi^k(P_{i+1}^k) - \psi^k(P_{i-1}^k)}{\| \overrightarrow{P_{i-1}^k P_{i+1}^k} \|}.$$

Then the displacement is given by

$$\overrightarrow{P_i^k P_i^{k+1}} = \Delta t \; \frac{\psi^k(P_{i+1}^k) - \psi^k(P_{i-1}^k)}{\| \overrightarrow{P_{i-1}^k P_{i+1}^k} \|}, \quad \text{for } i = 1, ..., I-1. \tag{3.9}$$

Formula (3.9) is only used if point P_i^k belongs to Ω. In addition, we solve equations (2.18) to determine the two points P_1^{k+1} and P_I^{k+1} of Γ_h^{k+1}, which belong to the boundary $\partial\Omega$. Again we use an explicit scheme to compute the displacement of the top and toe, yielding respectively

$$\overrightarrow{P_1^k P_1^{k+1}} = -\Delta t \; \frac{\psi^k(P_2^k)}{z(P_2^k)} \;\text{ and }\; \overrightarrow{P_I^k P_I^{k+1}} = \Delta t \; \frac{\psi^k(P_{I-1}^k)}{1 - z(P_{I-1}^k)}, \tag{3.10}$$

where $z(P)$ denotes the z-coordinate of point P.

To ensure stability of the numerical time integration we chose the time step such that the Courant-Friedrichs-Lewy (CFL) condition

$$\text{CFL} = C^k \frac{\Delta t}{l^k} \leq 1, \tag{3.11}$$

is satisfied at every time level k. Here, the constant C is given by

$$C^k = \max_{(x_i^k, z_i^k) \in \Gamma_h^k} \left\{ |\mathbf{q}(x_i^k, z_i^k)| \right\} = \max_{(x_i^k, z_i^k) \in \Gamma_h^k} \left\{ |q_x(x_i^k, z_i^k)|, |q_z(x_i^k, z_i^k)| \right\}, \tag{3.12}$$

and l^k denotes the minimum distance between two adjacent nodal points at the piecewise linear interface. For all practical purposes we chose CFL $= 0.2$.

4 The homogeneous case

The homogeneous case, i.e. when $\kappa_1 = \kappa_2 = \kappa$ in Ω, has been studied extensively by Chan Hong et.al. [6]. They parameterize the height of the interface and use the explicit $S^{\alpha,\beta}$-scheme of Lerat & Peyret [13] to discretize the hyperbolic interface motion equation (2.13). The parameters α, β are chosen such that they attain "optimal" values, with respect to the discretization of (2.13), see e.g. Wilders [20]. In addition they use a Runge-Kutta method to compute the displacement of the top and toe of the interface. For completeness and to gain confidence in the front tracking procedure proposed in this paper, we compare our numerical results with two distinct (semi) analytical similarity solutions of simplified problems: the rotating linear interface and slumping of brine mounds.

The full problem (2.17) can be reduced to a simplified problem, under the so called Dupuit approximation, yielding a nonlinear diffusion equation for the parameterized height of the interface. In this approximation, one assumes that the horizontal component of the specific discharge vector is constant in each fluid, and jumps at the interface. In view of $q_x = -\partial\Psi/\partial z$, this is equivalent to saying that the stream function is linear in z in each fluid. Numerical experiments, have shown that this is a reasonable approximation, as long as the inclination angle of the interface with the horizontal is less than $\pi/4$, provided the porous medium is homogeneous, see e.g. Chan-Hong et. al. [6]. Under the Dupuit approximation, interface motion equation (2.13) reduces to (after scaling according to (2.15), (2.16))

$$\frac{\partial u}{\partial t} = \frac{\partial}{\partial x}\left\{ \kappa\ u(1-u)\frac{\partial u/\partial x}{1+(\partial u/\partial x)^2} \right\} \quad \text{for} \quad (x,t) \in \mathbf{R}\times\mathbf{R}^+, \tag{4.1}$$

subject to the initial condition $u(x,0) = u_0(x)$, while the stream function is given by

$$\Psi(u,x,t) = \kappa\ u(1-u)\frac{\partial u/\partial x}{1+(\partial u/\partial x)^2}. \tag{4.2}$$

For homogeneous aquifers, κ is constant. Therefore, its appearance in equation 4.1 is not essential, but only there to keep the scaling uniform throughout the paper. These particular forms are due to De Josselin de Jong [11]. Note that (4.1) is only valid under the assumption that the interface extends through the full depth of the aquifer, hence $u \in [0,1]$. Equation is degenerate parabolic: at points where $u = 0,\ 1$ or $\partial u/\partial x = -1, +1$, the coefficient of the second-order derivative vanishes.

4.1 Comparison with the rotating line solution

The Dupuit equation (4.1) allows a similarity solution of the form

$$u_s(x,t) = \xi(\eta) \quad \text{with} \quad \eta = xg(t), \tag{4.3}$$

where the function ξ is given by

$$\xi(\eta) = \begin{cases} 0 & -\infty < \eta \le -\frac{1}{2} \\ \eta + \frac{1}{2} & -\frac{1}{2} < \eta < +\frac{1}{2} \\ 1 & +\frac{1}{2} \le \eta < +\infty \end{cases} \tag{4.4}$$

and where the function $g(t)$ is the solution of the initial value problem

$$\frac{dg}{dt} = -2\frac{g^3}{1+g^2} \quad \text{for} \quad t > 0, \tag{4.5}$$

subject to $g(0) = g_0$, see Zhang [23]. For $g_0 \in [-1,1]$ the similarity solution of (4.1) has the character of a rotating linear interface. It defines two interface curves in the (x,t)-plane: for $\eta = -1/2$ the movement of the toe is given by $(-1/(2g(t)), t)$ and for $\eta = +1/2$ the movement of the top is given by $(+1/(2g(t)), t)$. The similarity solution represents the large time behavior of equation (4.1). Van Duijn & Hilhorst [10] and Bertsch et al. [5] proved that an arbitrary initial interface converges towards u_s at $t \to \infty$. Chan Hong et. al. [6] demonstrated numerically similar behavior of the full problem. A highly irregular initial interface tends towards to a rotating linear interface as $t \to \infty$. Let the initial condition for u in problem (2.17)-(2.17) be given by

$$u_0(x) = \begin{cases} 0 & -1 \le x \le -\frac{1}{2} \\ x + \frac{1}{2} & -\frac{1}{2} < x < +\frac{1}{2} \\ 1 & +\frac{1}{2} \le x \le +1 \end{cases} \tag{4.6}$$

which corresponds to $g(0) = 1$ for the rotating line solution. In Figure 2 we compare the movement of the top and toe of the interface in the (x,t)-plane, for three different solutions: the (semi) explicit rotating line solution, a numerical solution based on the $S^{\alpha,\beta}$-scheme and a numerical solution based on the front tracking method. Note that both numerical solutions are indistinguishable on the scale of Figure 2: the maximum relative difference is $\approx 0.06\%$. With respect to the speed of propagation $\dot{S}(t)$ of the top and toe of the interface we observe in Figure 2 convergence of the numerical solutions (a,b,d and e) towards the similarity solution (c and f). The numerically computed positions of the top and toe converge 'up to a constant' towards the Dupuit similarity solution.

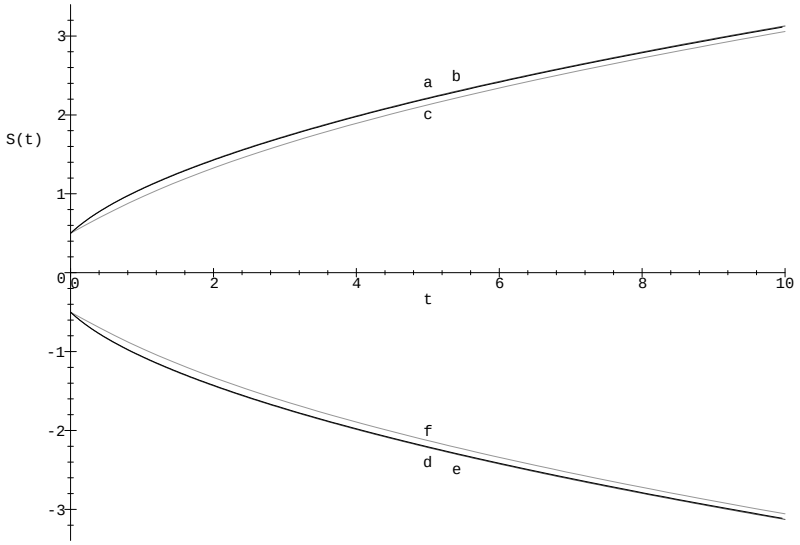

Figure 2. Comparison of the time evolution of the top and toe: (a) and (f) front tracking method, (b) and (e) $S^{\alpha,\beta}$-scheme, (c) and (f) the Dupuit similarity solution.

4.2 Bounds on the time scale of slumping brine mounds

Equation (4.1) only applies to special configurations with fresh-salt interfaces extending through the full depth of an aquifer confined top and bottom by impermeable horizontal boundaries. When the initial interface shape takes the form of a two-dimensional brine mound of finite volume, Van Duijn & Philip [17] in their analytical study show that (4.1) may be replaced by

$$\frac{\partial u}{\partial t} = \frac{\partial}{\partial x}\left(u\frac{\partial x}{\partial x}\right) \quad \text{for} \quad (x,t) \in \mathbf{R}\times\mathbf{R}^{+}, \tag{4.7}$$

under the assumption that $(\partial u/\partial x)^2 << 1$ and $u << 1$. This equation has a parabolic similarity solution, given by

$$u(x,t) = \begin{cases} \left(\dfrac{3a^2}{32(t+T)}\right)^{\frac{1}{3}} - \dfrac{x^2}{6(t+T)} & \text{for} \quad |x| \le \left(\dfrac{9a(t+T)}{2}\right)^{\frac{1}{3}} \\ 0 & \text{for} \quad |x| > \left(\dfrac{9a(t+T)}{2}\right)^{\frac{1}{3}} \end{cases} \tag{4.8}$$

where the constant T is defined by

$$T = \frac{3a^2}{32(u(0,0))^3}. \tag{4.9}$$

This solution describes nonlinear diffusion of an instantaneous source of strength a, released at $t = 0$, and has been obtained independently by Barenblatt [1] and Pattle [15]. Van Duijn & Philip [17] show that this solution gives a lower bound on the time scale of slumping brine mounds.

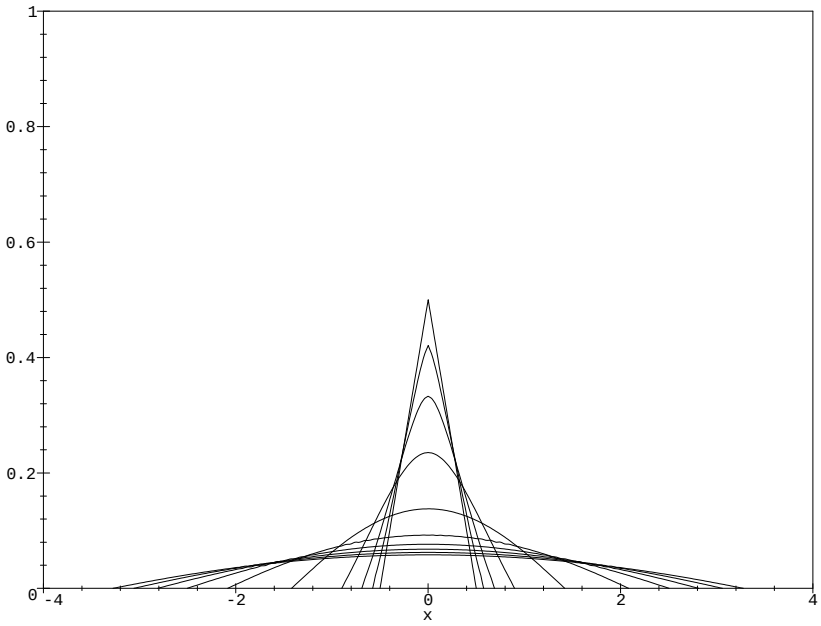

Figure 3.a. Computed time evolution of a decaying brine mound.

Moreover, they derive an approximate interface motion equation that gives a upper bound on the time scale of the slumping slumping process. Equation (4.1) is modified to restrict the fluid motion to the region $0 \leq z \leq g(t)^{-1}$, yielding

$$\frac{\partial u}{\partial t} = \frac{\partial}{\partial x}\left\{ u(g^{-1} - u)\frac{\partial u/\partial x}{1 + (\partial u/\partial x)^2} \right\}, \tag{4.10}$$

where $g(t)$ is a priori unknown and emerges as a part of the similarity solution of the problem. In writing (4.10), one implicitly assumes that fluid above the plane $\{z = g(t)\}$ is at rest. A triangular brine mound preserves mass and produces similarity when the horizontal dimensions increase by the factor $g(t)$ and vertical dimensions decrease by the factor $1/g(t)$. The function $g(t)$ is implicitly given by

$$t = \ln\left(\frac{g}{g_0}\right) + \frac{a^2}{4}(g^4 - g_0^4), \tag{4.11}$$

where $g_0 = g(0)$. For the details we refer to [17]. The gravitational potential energy is proportional to the elevation of the mound centre of gravity above its base. This quantity is used to match the triangular (Δ) and parabolic ($\cap$) similarity solutions appropriately. One easily verifies that

$$\bar{z}_\Delta(t) = \frac{1}{3g(t)} \quad \text{and} \quad \bar{z}_\cap(t) = \left(\frac{3a^2}{500}\right)^{\frac{1}{3}} \frac{1}{(t+T)^{\frac{1}{3}}}. \tag{4.12}$$

Matching these expressions at $t = 0$ yields

$$u_\cap(0,0) = \left(\frac{125}{144}\right)^{\frac{1}{3}} \frac{1}{g(0)} \quad \text{and} \quad T = \frac{27}{250}a^2 g(0)^{\frac{1}{3}}. \tag{4.13}$$

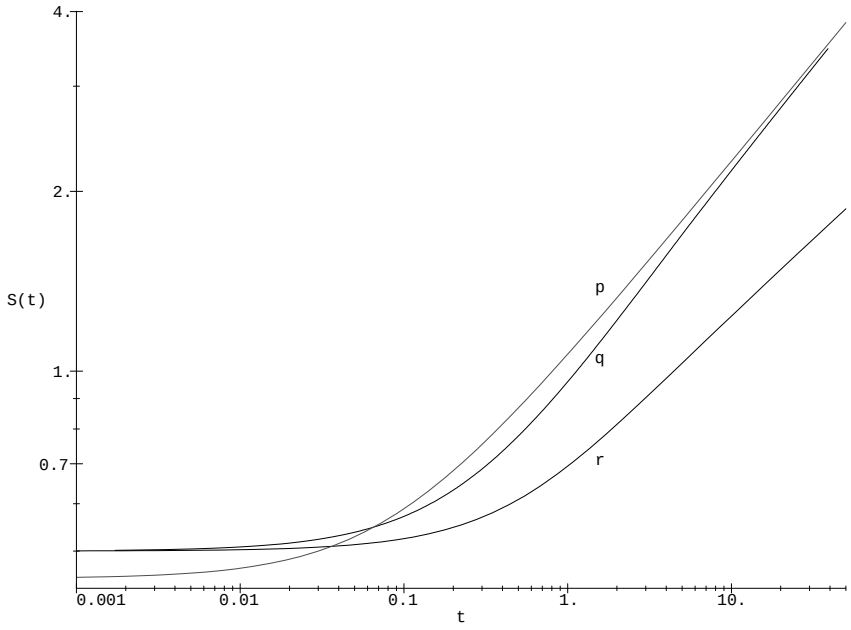

Figure 3.b. Time evolution of the toe: Lower bound on the time scale (p), i.e. parabolic solution, the numerical solution (q) and upper bound (r), i.e. triangular solution.

The time course of the semi-width of the mound at its base, i.e. the position of the mound toe $S(t)$ at the right-hand side, for respectively the triangular and parabolic solution are given by

$$S_\Delta(t) = ag = \frac{a}{3\bar{z}_\Delta(t)} \quad \text{and} \quad S_\cap(t) = \left(\frac{9a(t+T)}{2}\right)^{\frac{1}{3}} = \frac{3a}{10\bar{z}_\cap(t)}. \tag{4.14}$$

The upper bound on the time scale (i.e. a lower bound on the displacement scale) is given by $t(S_\Delta)$ and the lower bound by $t(S_\cap)$. The computed time evolution of a brine mound, initially given by

$$u_0(x) = \begin{cases} \frac{1}{2} - x & \text{for} \quad 0 \le x \le \frac{1}{2} \\ \frac{1}{2} + x & \text{for} \quad -\frac{1}{2} \le x < 0 \\ 0 & \text{for} \quad |x| > \frac{1}{2} \end{cases} \tag{4.15}$$

is shown in Figure 3.a. In Figure 3.b. we compare the bounds on the time scale obtained by Van Duijn & Philip [17] with a numerical solution of the full problem. Observe that the behavior of the numerical solution is closer to the upper bound (Δ) at the (very) short time scale, while it approaches the lower bound ($\cap$) at large t. This is exactly the behavior that was predicted in [17].

5 An interface crossing a discontinuity in permeability

When a fresh-salt interface intersects a discontinuity in permeability, it is possible to derive a simple expression for the shape of the interface in an infinitesimal small neighborhood of the intersection point, provided the interface

is non-singular. The derivation is based on the two-fluid interface conditions in a homogeneous porous medium combined with the flow conditions of a homogeneous fluid at a discontinuity in permeability. First we consider

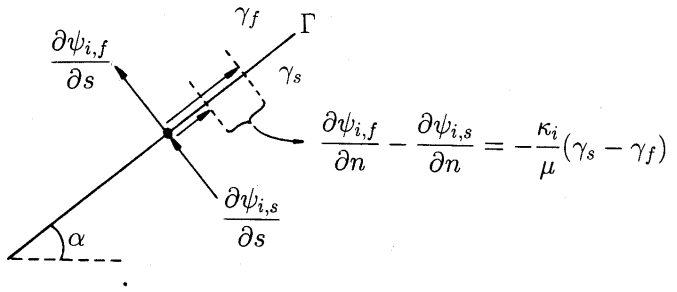

Figure 4. The shear flow at the interface.

a linear interface Γ, under an inclination angle α with the horizontal, separating two fluids with specific weights γ_f (upper fluid) and γ_s (lower fluid). At the interface, the normal components of the specific discharge are continuous, i.e.

$$\frac{\partial \psi_{i,f}}{\partial s} = \frac{\partial \psi_{i,s}}{\partial s} \quad \text{for} \quad i = 1, 2 \tag{5.1}$$

while the tangential components of the specific discharge satisfy the shear flow relation, given by

$$\frac{\partial \psi_{i,f}}{\partial n} - \frac{\partial \psi_{i,s}}{\partial n} = -\frac{\kappa_i}{\mu}(\gamma_s - \gamma_f)\sin(\alpha) \quad \text{for} \quad i = 1, 2, \tag{5.2}$$

see Figure 4. Then the corresponding relations between the x- and z-components of the specific discharge are given by

$$-\frac{\partial \psi_{i,f}}{\partial z} + \frac{\partial \psi_{i,s}}{\partial z} = \frac{\kappa_i}{\mu}(\gamma_s - \gamma_f)\sin(\alpha)\cos(\alpha) \quad \text{for} \quad i = 1, 2, \tag{5.3}$$

and

$$\frac{\partial \psi_{i,f}}{\partial x} - \frac{\partial \psi_{i,s}}{\partial x} = \frac{\kappa}{\mu}(\gamma_s - \gamma_f)\sin^2(\alpha) \quad \text{for} \quad i = 1, 2. \tag{5.4}$$

Next we consider flow of a homogeneous fluid in the vicinity of a discontinuity in permeability Σ, separating two regions with different intrinsic permeability: κ_1 (upper region) and κ_2 (lower region). The inclination angle between the discontinuity and the horizontal is given by β. Again we require continuity of the specific discharge components normal to the discontinuity in κ, hence

$$\frac{\partial \psi_{1,j}}{\partial s} = \frac{\partial \psi_{2,j}}{\partial s} \quad \text{for} \quad j = f, s, \tag{5.5}$$

while the tangential discharge components at the discontinuity satisfy

$$\kappa_2 \frac{\partial \psi_{1,j}}{\partial n} - \kappa_1 \frac{\partial \psi_{2,j}}{\partial n} = 0 \quad \text{for} \quad j = f, s, \tag{5.6}$$

see Figure 5. Consequently the relations between the x- and y-components of the specific discharge are given by

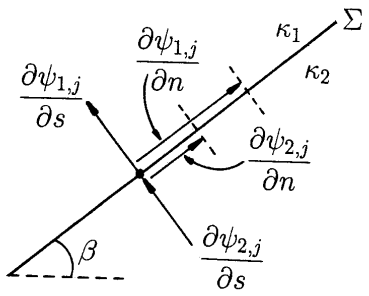

Figure 5. The discharge components at a discontinuity in permeability.

$$\tan(\beta)\left(-\frac{\partial \psi_{1,j}}{\partial z}+\frac{\partial \psi_{2,j}}{\partial z}\right)=\left(\frac{\partial \psi_{1,j}}{\partial x}-\frac{\partial \psi_{2,j}}{\partial x}\right) \quad \text{for} \quad j=f,s, \tag{5.7}$$

and

$$\kappa_1\frac{\partial \psi_{2,j}}{\partial z}-\kappa_2\frac{\partial \psi_{1,j}}{\partial z}=\left(\kappa_1\frac{\partial \psi_{2,j}}{\partial x}-\kappa_2\frac{\partial \psi_{1j}}{\partial x}\right)\tan(\beta) \quad \text{for} \quad j=f,s. \tag{5.8}$$

Expressions (5.3), (5.4) and (5.7), (5.8) can be combined in the following way. Consider a straight line through the origin of the (x,z)-plane, under inclination angle β with the horizontal x-axis, being a vertical cross section of the plane separating two regions with permeability κ_1 (upper region) and κ_2 (lower region). A sharp interface, separating two fluids with specific weight γ_f (upper fluid) and γ_s (lower fluid), intersects this line in the origin. The inclination angle of the interface with the horizontal in the region $x>0$ is denoted by α_1, while the angle between the interface and the negative x-axis, i.e. in the region $x<0$, is given by α_2. We assume for the moment that $\alpha_1 \neq \alpha_2 \neq \beta$, implying that interface and discontinuity in permeability divide the (x,z)-plane in four distinct regions. Provided the interface is non-singular (finite and compatible velocities), the discharge components in an infinitesimal small neighborhood of the origin, between adjacent regions, have to satisfy (5.3), (5.4) or (5.7), (5.8). Hence, given the x- and z-discharge components in one of the regions, we can compute all corresponding discharges in the other regions. After some elementary algebra we obtain

$$\tan(\alpha_1)=\frac{\tan(\alpha_2)\left(1+\frac{\kappa_1}{\kappa_2}\tan^2(\beta)\right)-\left(1-\frac{\kappa_1}{\kappa_2}\right)\tan(\beta)}{\left(\frac{\kappa_1}{\kappa_2}+\tan^2(\beta)\right)-\tan(\alpha_2)\tan(\beta)\left(1-\frac{\kappa_1}{\kappa_2}\right)}. \tag{5.9}$$

A similar relation has been found by Bear & Shapiro [3], expressing the angles of intersection α_1 and α_2 in terms of β and the fresh and salt water fluxes in the intersection point. Note that the fluid density difference does not appear in (5.9).

In the limit $\kappa_1/\kappa_2 \to 1$, i.e. a homogeneous porous medium, (5.9) yields $\alpha_1=\alpha_2$, as to be expected. In case of a horizontal discontinuity in permeability, i.e. in the limit $\beta \to 0$, we obtain

$$\tan(\alpha_1)=\frac{\kappa_2}{\kappa_1}\tan\alpha_2 \tag{5.10}$$

while for a vertical discontinuity in permeability, i.e. in the limit $\beta \to \pi/2$, expression (5.9) reduces to

$$\tan(\alpha_1)=\frac{\kappa_1}{\kappa_2}\tan(\alpha_2). \tag{5.11}$$

The case $\beta = 0$, i.e. expression (5.10), implies that if $\alpha_1 \to \pi/2$ then $\alpha_2 \to \pi/2$. Equation (5.9) gives an exact relation between the angles of intersection and therefor it is an indispensable tool for computer code verification. Moreover it gains insight in the (transient) behavior of an interface intersecting a discontinuity in permeability.

6 Vertical discontinuity in permeability: the Dupuit approximation

For the special case of a vertical discontinuity in permeability, the scaled coefficient κ is given by

$$\kappa = \kappa(x) = \begin{cases} \kappa_1 & \text{for} \quad x < 0 \\ \\ \kappa_2 & \text{for} \quad x > 0 \end{cases} \tag{6.1}$$

Under the assumption that $\partial u/\partial x << 1$, i.e. in case of a (very) flat interface, equation (4.1) reduces to

$$\frac{\partial u}{\partial t} = \frac{\partial}{\partial x}\left\{\kappa(x)u(1-u)\frac{\partial u}{\partial x}\right\} \quad \text{for} \quad (x,t) \in \mathbf{R} \times \mathbf{R}^+ xi, \tag{6.2}$$

while the stream function is given by

$$\Psi(u,x,t) = \kappa(x)u(1-u)\partial u/\partial x \tag{6.3}$$

Continuity of the stream function at the discontinuity in κ at $x = 0$ requires

$$\lim_{x \downarrow 0} \Psi(u(x,t),x,t) = \lim_{x \uparrow 0} \Psi(u(x,t),x,t) \quad \text{for} t > 0. \tag{6.4}$$

In this limit (6.3) yields

$$\frac{\partial u}{\partial x}(0^+,t) = \left(\frac{\kappa_1}{\kappa_2}\right) \frac{\partial u}{\partial x}(0^-,t) \quad \text{or} \quad \tan(\alpha_1) = \left(\frac{\kappa_1}{\kappa_2}\right)\tan(\alpha_2). \tag{6.5}$$

This is identical to the exact expression (5.11). Note that the latter does not hold when $(\partial u \partial x)^2$ is not disregarded in (4.1).

Let the initial interface be given by

$$u(x,0) = u_0(x) = \begin{cases} 1 & \text{for} \quad x > 0 \\ 0 & \text{for} \quad x < 0 \end{cases} \tag{6.6}$$

Then, problem (6.2)-(6.6) allows a similarity transformation of the form

$$u(x,t) = f(\eta) \quad \text{with} \quad \eta = \frac{x}{\sqrt{t}}, \tag{6.7}$$

where the function f is a solution of the boundary value problem

$$\frac{1}{2}\eta f' + (\kappa(\eta)\ f(1-f)f')' = 0 \quad \text{for} \quad \eta \in \mathbf{R}, \tag{6.8}$$

where the primes denote differentiation with respect to η, subject to

$$f(-\infty) = 0 \quad \text{and} \quad f(+\infty) = 1. \tag{6.9}$$

The solution of this problem exhibits a jump in the derivative at $\eta = 0$. To eliminate this discontinuity we introduce a new variable according to

$$s(\eta) = \int_0^\eta \frac{1}{\kappa(\xi)}\, d\xi \quad \text{for} \quad \eta \in \mathbf{R}. \tag{6.10}$$

Because $\kappa(x)$ is piecewise constant, we may write

$$s(\eta) = \begin{cases} \eta/\kappa_1 & \text{for} \quad \eta < 0 \\ \eta/\kappa_2 & \text{for} \quad \eta > 0 \end{cases} \quad \text{or} \quad \kappa(s) = \begin{cases} \kappa_1 & \text{for} \quad s < 0 \\ \kappa_2 & \text{for} \quad s > 0 \end{cases} \tag{6.11}$$

Substitution of (6.11) in (6.8) yields

$$\frac{1}{2} s\kappa_2 f' + (f(1-f)f')' = 0 \ \text{ for } \ s > 0, \tag{6.12}$$

$$\frac{1}{2} s\kappa_1 f' + (f(1-f)f')' = 0 \ \text{ for } \ s < 0, \tag{6.13}$$

where the primes denote differentiation with respect to s. Now, the derivative f' is continuous at $s = 0$. Finally we introduce an additional transformation, in order to obtain the ratio κ_1/κ_2 as a single parameter in (6.12)-(6.13). Let

$$\xi = s\sqrt{\kappa_2} \ \text{ for } \ s \in \mathbf{R}, \tag{6.14}$$

then (6.12), (6.13) reduce to

$$\frac{1}{2} \xi f' + (f(1-f)f')' = 0 \ \text{ for } \ \xi > 0, \tag{6.15}$$

$$\frac{1}{2} \left(\frac{\kappa_1}{\kappa_2} \right) \xi f' + (f(1-f)f')' = 0 \ \text{ for } \ \xi < 0, \tag{6.16}$$

where now the primes denote differentiation with respect to ξ.

We solve boundary value problem (6.15), (6.16) subject to (6.9) numerically, using a shooting procedure in the sub-domains $\xi > 0$ and $\xi < 0$. The numerical integration is established with a standard adaptive step size Runge-Kutta method. First we solve (6.15) subject to $f(0) = f_0$ and $f'(0) = \alpha$, in the domain $\xi > 0$, where α denotes a shooting parameter. The value of α is determined experimentally, such that the numerical approximation of $f(\xi)$ satisfies the boundary condition $f(+\infty) = 1$. Next we solve (6.16) subject to f_0 and $f_0' = \alpha$ (α known), in the domain $\xi < 0$. In order to satisfy the boundary condition $f(-\infty) = 0$, we adjust the value of the ratio κ_1/κ_2 accordingly in (6.16). Equations (6.15), (6.16) imply that f_0, which corresponds to the (stationary) height of the interface at $x = 0$ for any $t > 0$, depends on the ratio κ_1/κ_2 only. Figure 6 shows the numerical results for $f_0 = f_0(\kappa_1/\kappa_2)$.

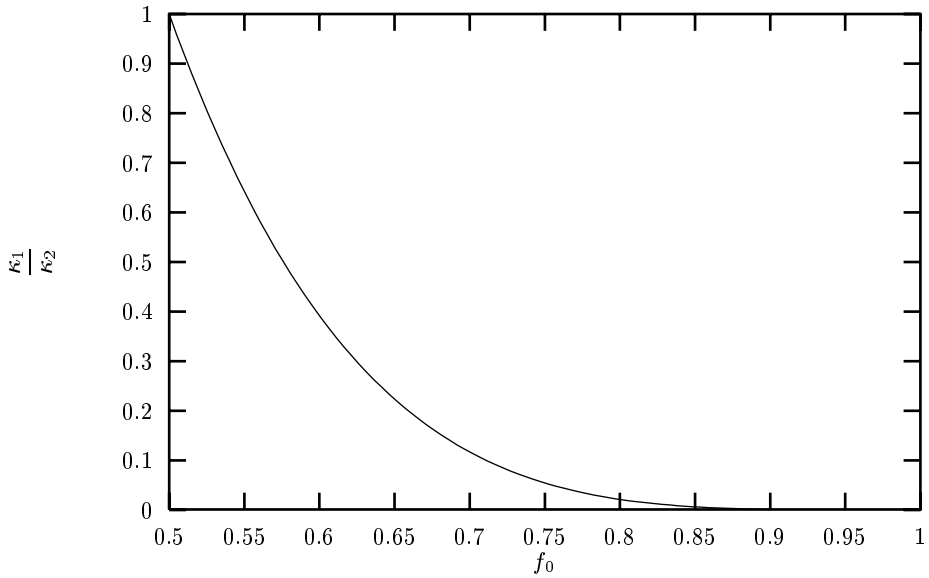

Figure 6. The relation between f_0 and κ_1/κ_2, for $0.5 < f_0 < 1.0$

When $\kappa_1/\kappa_2 = 1$, equations (6.12)-(6.13) reduce to (6.15), but now for $\xi \in \mathbf{R}$. The latter has an exact solution of the form of a rotating line, given by

$$f(\xi) = \begin{cases} 1 & \text{for} \quad \xi > 0 \\ \frac{1}{2}(1+\xi) & \text{for} \quad -1 \le \xi \le +1 \\ 0 & \text{for} \quad \xi < -1 \end{cases} \tag{6.17}$$

see Philip [16]. Figure 7 shows numerical approximations of the similarity solution $f(\xi)$ for different values of the ratio κ_1/κ_2. Figure 8 gives an example of the time evolution of the interface $u(x,t)$ for $\kappa_1/\kappa_2 = 0.1261$ and $f_0 = u(0,t) = 0.7$.

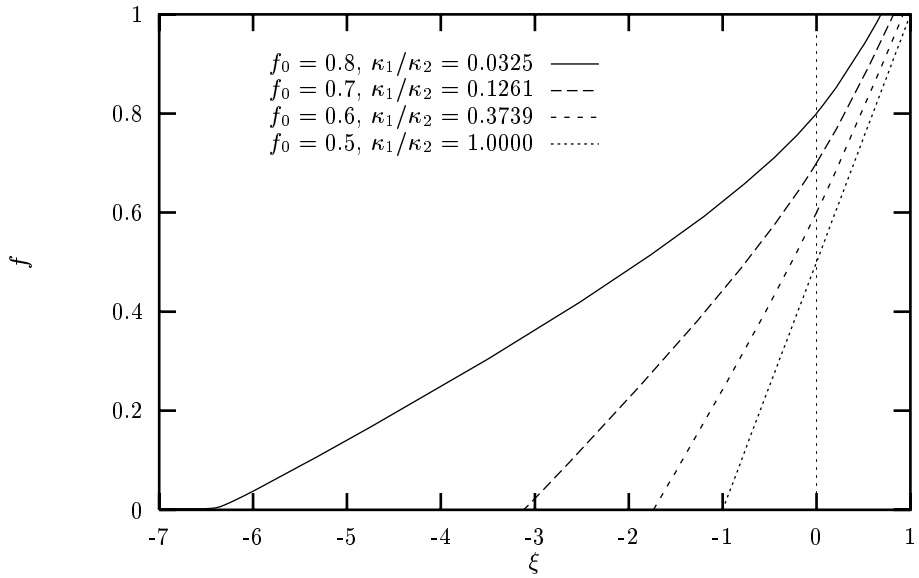

Figure 7. The similarity solution $f(\xi)$ for different values of f_0 and corresponding κ_1/κ_2-values

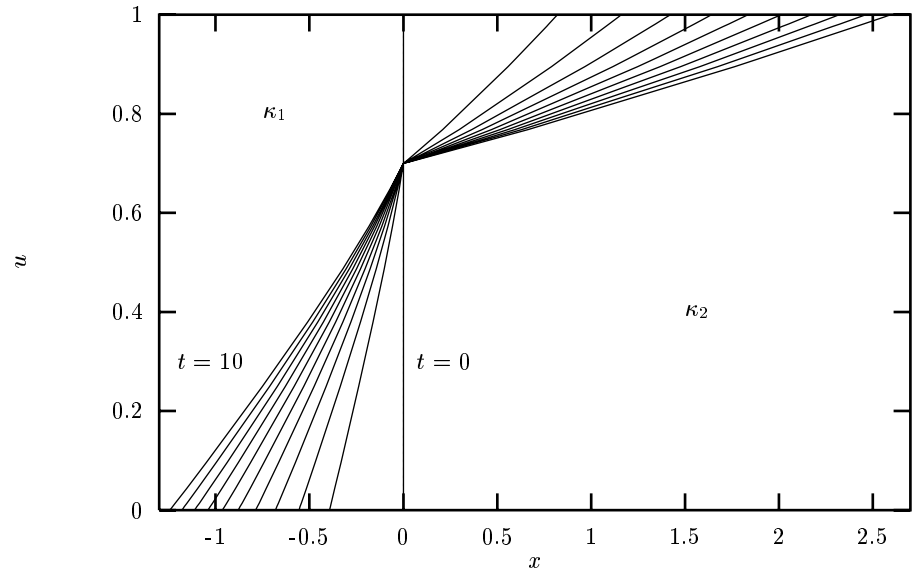

Figure 8. An example of the time evolution of an interface crossing a vertical discontinuity in permeability: the similarity solution for $\kappa_2 = 1.0$, $\kappa_1 = 0.1261$ and $f_0 = 0.7$. The time levels are $t = 0, 1, 2...10.0$.

In Figure 9 we show the numerical solution for $\kappa_1/\kappa_2 = 0.1261$ ($f_0 = 0.7$) in terms of the similarity variable $\eta = x/\sqrt{t}$. The result clearly demonstrates the convergence of the numerical solution towards a similarity

solution. The corresponding Dupuit similarity solution is also shown in Figure 9 (the dashed line). Notice the small difference between the numerically obtained similarity solution and the approximate Dupuit solution.

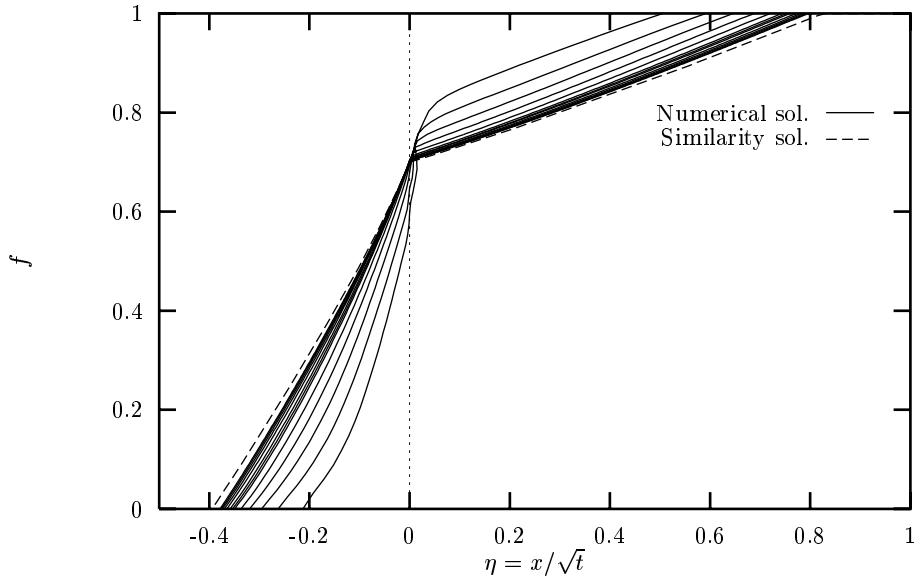

Figure 9. Convergence of the numerical solution towards a similarity solution. The dashed line represents the Dupuit similarity solution

The approximate Dupuit solution satisfies (5.11) for all $t > 0$, see also (6.4), (6.5). To check whether (5.11) is satisfied by the numerical solution we define the relative error $F = (1 - \kappa_2 \tan(\alpha_1^k)/(\kappa_1 \tan(\alpha_2^k))) \cdot 100\%$, where α_1^k and α_2^k denote the computed angles of intersection at time $t = t^k$. The time evolution of F is depicted in Figure 10. Each plot marker corresponds to a certain time level; intermediate time levels have been omitted. For short times we find large deviations between the computed results and expression (5.11). This is due to the singular behavior of the interface at the very short time scale of the computations, see Figure 9. As time proceeds, the relative error F tends towards a limiting value: $F \approx -0.6\%$.

The time evolution of the speed of propagation of the top and toe of the interface is shown in Figure 11. Again, we observe convergence of the numerically computed speeds towards the speeds computed with the Dupuit solution.

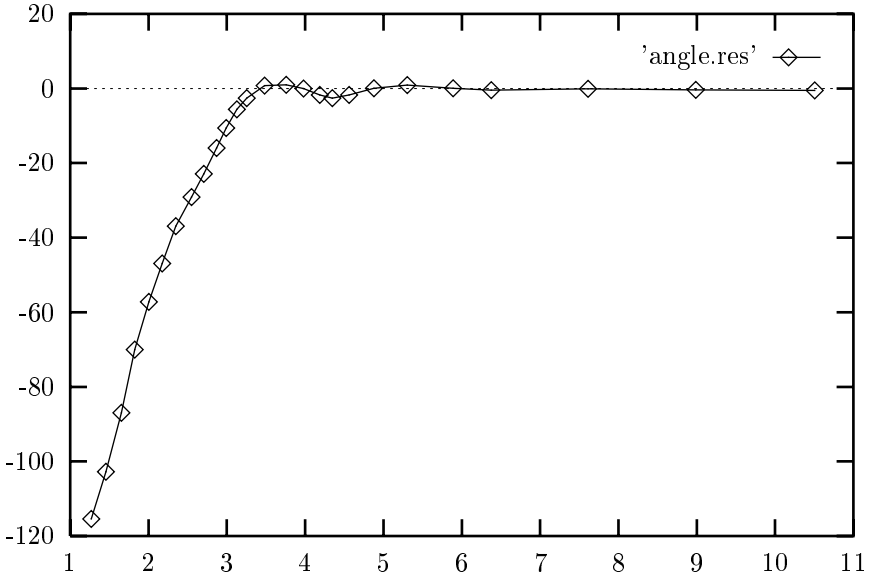

Figure 10. The relative error F as a function of time.

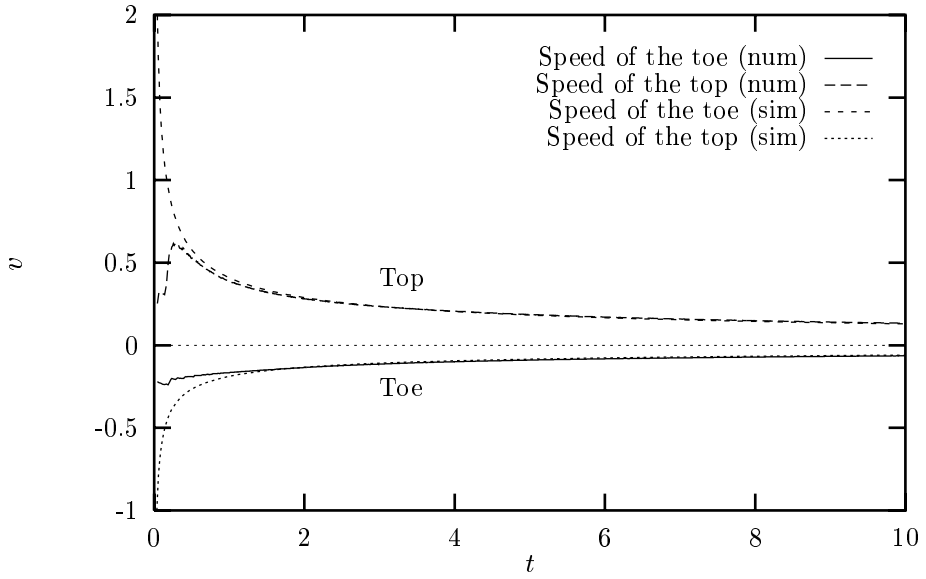

Figure 11. Time evolution of the speed of propagation of the top and toe of an interface: comparison of the numerical and similarity solutions.

7 A horizontal discontinuity in permeability

Next we consider a horizontal heterogeneity, consisting of two parallel layers of equal thickness with different permeability κ_1 (upper layer) and κ_2 (lower layer), under the assumption that $\kappa_1 < \kappa_2$. The initial interface is vertical at $x = 0$, such that the region $x < 0$ is occupied by fresh water and the region $x > 0$ by salt water. In this more complicated case it is not possible to obtain a similarity solution of a simplified problem based on the Dupuit approximation. If we assume that the two regions are separated at the plane $\{z = 1/2\}$ by an impermeable sheet, and apply the Dupuit approximation in both regions, we obtain two independent rotating line solutions. However, this is far from realistic because the exchange of fluid between the layers is disregarded.

For $t > 0$, a hydrodynamically instable zone, i.e. salt water on top of fresh water, develops in the vicinity of the discontinuity in permeability. The horizontal width of this zone grows in time. Under natural (field) conditions, small local variations in permeability perturb the interface in this zone, and fresh-salt fingers may occur. These fingers grow in time. The linear stability analysis shows that fingers of any width or 'wave length' > 0 can develop. The distribution of wave lengths in the fingering pattern depends upon the nature of the perturbation mechanism of the interface, e.g. the local (small scale) heterogeneous permeability field.

When we consider fresh and salt groundwater as miscible fluids and allow for diffusion/dispersion, stability analysis showed that there exists a (minimum) critical wave length λ_0 in the fingering pattern. The value of λ_0 is related to the value of the diffusivity/dispersivity D, see for instance List [14]. This implies that fingers with width smaller than (half) the critical wave length are dissipated by diffusion and/or dispersion and decay in time. In case of the interface approximation, i.e. in the limit $D \to 0$, we have, at least in theory, $\lambda_0 = 0$.

The computed time evolution of an initially vertical interface exhibits the development of fresh-salt fingers in the vicinity of the horizontal discontinuity in permeability, see Figure 12. To ensure numerical stability, the (variable) time step is chosen such that the condition CFL$= 0.2$ is satisfied at any time level. The onset of the instabilities in the physically unstable zone is caused by the discrete approximation of the interface: small numerical and discretization errors perturb the unstable interface at any time level which triggers the growth of the fresh-salt fingers.

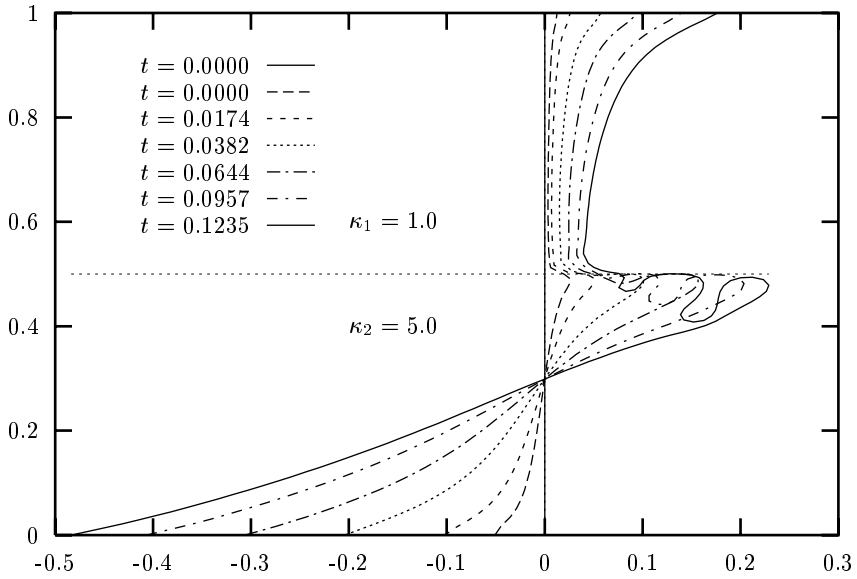

Figure 12. Time evolution of an initially vertical interface.

The width of the fingers that grow in time is directly related to the coarseness of the discretization of the interface. The minimum finger width at the onset of an instability is approximately 6 interface piecewise linears. If we refine the mesh by a factor 2, the width of the fingers that grow is also reduced by a factor 2, while the fingers start to develop earlier. In Figure 13, we compare two interfaces at $t = 0.1235$. The dashed line corresponds to the last interface shown in Figure 12, and is computed with a fine mesh. The solid line is the result of a computation with a coarse mesh, i.e. the number of nodal points at the interface is reduced by a factor 2when compared to the fine mesh. The computations break down when adjacent parts of the interface coincide. The discretization of the flow domain, i.e. two distinct regions separated by a single interface, does not allow the formation of salt or fresh water drops. The latter implies that only the short time development of instabilities can be simulated with this numerical approach.

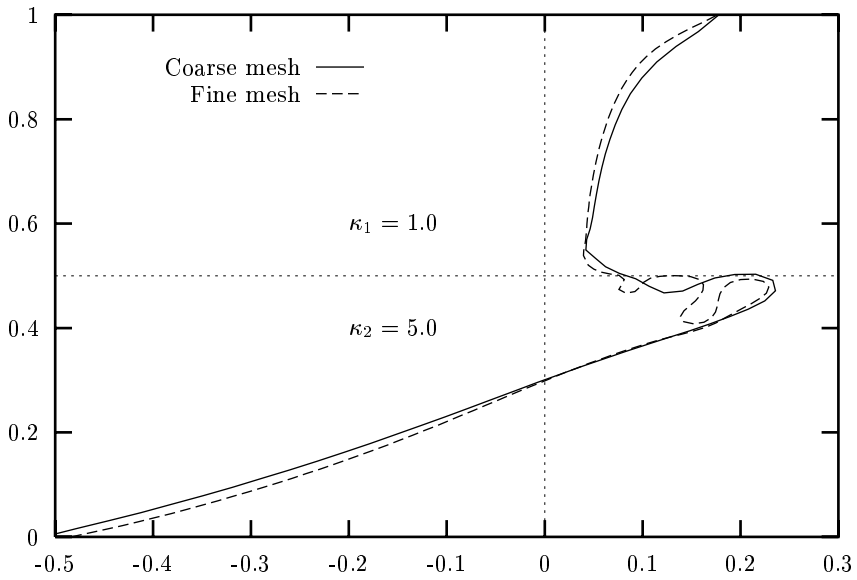

Figure 13. Interfaces at $t = 0.1235$, computed with a fine and a coarse discretization.

In Figure 14 we show the time evolution of an initially horizontal interface which coincides with the discontinuity in permeability. This interface is perturbed at $(0, 0.5)$ by -0.006. The upper part of the flow domain, i.e. the region where $\kappa_1 = 0.5$, is filled with salt water, and the lower part, i.e. the region where $\kappa_2 = 1.0$ is filled with

fresh water. The computed finger shapes are not very smooth: the individual piecewise linears are clearly visible. The latter will always be that case. If we refine the mesh, the finger widths reduce accordingly. The asymmetry of the fingering pattern is caused by the asymmetry of the generated meshes with respect to the z-axis. If we do not perturb the initially horizontal interface, no growth of instabilities is observed, as to be expected. The initial interface is perfectly horizontal and the velocity field remains identically zero for all times.

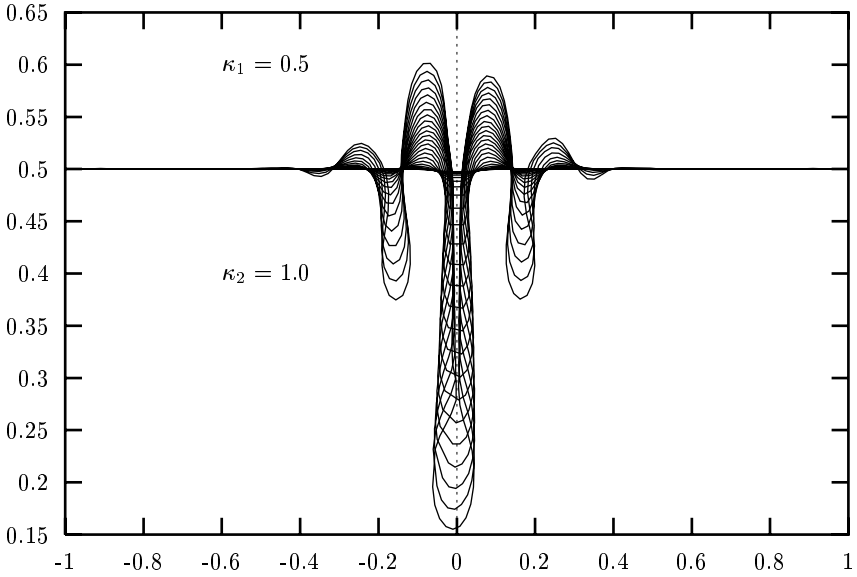

Fig 15. Time evolution of an initially horizontal interface that coincides with the discontinuity in permeability, and which is perturbed at (0.0,0.5) by -0.006.

A similar computation was carried out for the homogeneous case. The time evolution is shown in Figure 15. An example of the triangularization of the salt water domain is given in Figure 16. Notice the refinement of the discretization in the vicinity of the interface.

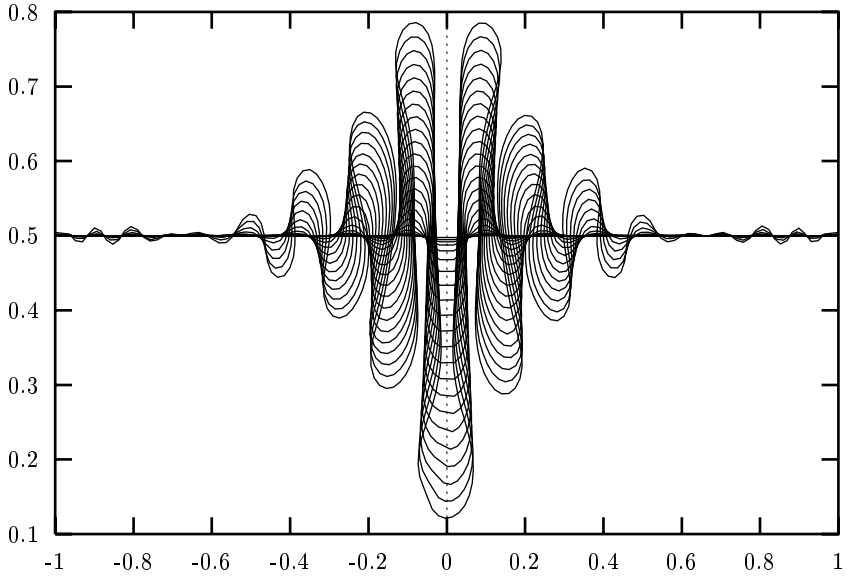

Figure 15. Time evolution of an initially horizontal interface which is perturbed at $(0.0, 0.5)$ by -0.006.

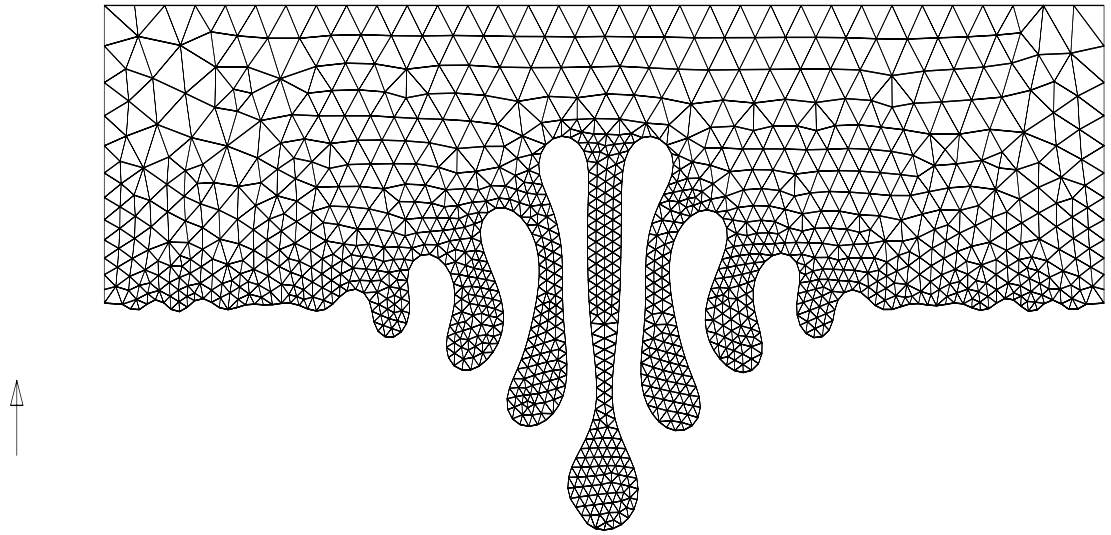

Figure 16. Triangularization of the salt water region

8 Discussion and conclusions

The proposed front tracking procedure gives results within the same range of accuracy as the predictor-corrector scheme used by Chan Hong et. al. [6]. At least for parametrizable interfaces ($z = u(x,t)$) we are able to show this convincingly by comparison of results, generated with both methods. See for instance the rotating linear interface in a homogeneous flow domain in Section 4.1. For multivalued interfaces, no reliable test problems or related approximate Dupuit problems are available.

The bounds on the time scale of slumping brine mounds, as predicted by Van Duijn & Philip [17], could be verified and confirmed. The triangular Dupuit solution predicts the short-time behavior of the numerical solution of the full problem, while the parabolic Dupuit solution describes the large-time behavior. These results emphasize the utility of the Dupuit assumption in solving practical interface problems.

When an interface crosses a discontinuity in permeability, an exact expression can be derived, which relates the contrast in permeability to the angles of intersection at the discontinuity, see (5.9). If, given a permeability ratio κ_1/κ_2, the angles of intersection do not satisfy this expression, the velocities at the point of intersection will be, at least theoretically, singular. Indeed, very high velocities are encountered at the short-time scale of computations. As time proceeds, the computed interface shapes at the discontinuity in permeability converge towards the shape predicted by expression (5.9). In fact, the initially vertical interface, i.e. the initial condition for all heterogeneous computations, is singular itself due to the kinks at the domain boundaries. This also leads to very high initial velocities, and accordingly, due to the CFL constraint on the time step, to very small (initial) time steps.

For the case of a vertical discontinuity in permeability, a related approximate Dupuit could be solved in terms of a (semi) explicit similarity solution. The numerical solution of the full problem also converges towards a similarity profile as $t \to \infty$. The Dupuit solution gives a reasonable approximation of the large-time behavior of the numerical solution. Whereas the similarity profiles are not completely identical, the velocities of the top and toe of both solutions converge towards the same limiting values (up to small error).

The width of the fresh-salt fingers that occur in the unstable regions is selected by the numerical method, and not by any physical mechanism. This is a direct consequence of the absense of diffusion/dispersion in the interface approximation. Refinement of the mesh at the interface leads to smaller finger widths. This implies that the practical applicability of interface models for simulation of instabilities is limited. Moreover, the instabilities or fingers create a mixing zone of fresh and salt groundwater which is in some sense in contradiction with the

interface approximation: strictly miscible fluids are considered to be immiscible.

References

[1] Barenblatt, G.I. *On some unsteady motions of a liquid and a gas in a porous medium*, Akad. Nauk. SSSR Prikl. Math. Mekh. **16**, pp 67-78.

[2] J. Bear. *Dynamics of fluids in porous media*, 1975, New York, American Elsevier.

[3] Bear, J. & Shapiro, A.M. *On the shape of the non-steady interface intersecting discontinuities in permeability* , Adv. Water Resources, Volume **7** (1984), pp. 106-112.

[4] J. Bear. *Hydraulics of groundwater*, 1979, New York, McGraw-Hill.

[5] Bertsch, M, Esteban, J.R. & Zhang, H. *On the asymptotic behaviour of solutions of a degenerate equation in hydrology* , Nonlinear Anal., Theor. Meth. & Appl. **19** (1992), p.p. 365-374.

[6] J.R. Chan Hong, C.J. van Duijn, D. Hilhorst, J. van Kester. *The interface between fresh and salt groundwater : a numerical study*, IMA J. of Appl. Math. (1989), 42, 299-316.

[7] C. Dupaix, D. Hilhorst, J.F. Scheid. *On a dissolution-growth problem with surface tension : a numerical study*, to appear.

[8]

[9] Van Duijn, C.J. $ De Josselin De Jong, G. *Free boundary problems in fresh-salt groundwater flow*, In Summer School on Flow and Transport in Porous Media, Beijing, China, 8-26 August 1988, Editor: Xiao Shutie, World Scientific.

[10] Van Duijn, C.J. & Hilhorst, D. *On a doubly nonlinear diffusion equation in hydrology*, Nonlinear Anal. Theory Meth. Appl. **11**, 305-333.

[11] De Josselin De Jong, G. *The simultaneous flow of fresh water in aquifers of large horizontal extension determined by shear flow and vortex theory*, Proceedings Euromech. **143** (1981) (eds A. Verruijt & F.B.J. Barends), Balkema Rotterdam, pp. 132-149.

[12] De Josselin De Jong, G. *Singularity distributions for the analysis of multiple flow through porous media*, J. Geophys. Res. **65** (1960), p.p. 3739-3758.

[13] Lerat, A. & Peyret, R *Sur le chois de schémas aux différences finies du second ordere fournissant des profiles de choc sans oscillations.* C.R. Acad. Sci. Paris **277** (1973), pp. 363-366.

[14] List, E.J. *The stability and mixing of a density-stratified horizontal flow in a porous medium*, Rep. KH-R-11, Calif. Inst. of Technology, Pasadena (1965).

[15] Pattle, R.E. *Diffusion from an instantaneous point source with a concentration dependent coefficient*, Q.J. Mech. Appl. Mech. **12** (1959), pp. 407-409.

[16] Philip, J.R. *Diffusion from an instantaneous point source with a concentration dependent coefficient* , Q.J. Mech. Appl. Mech. 12 (1959), p.p. 407-409.

[17] Philip, J.R. & Van Duijn, C.J. *Slumping of brine mounds: bounds on behaviour*, Journal of Hydrology **179** (1996), pp. 159-180.

[18] Scheid, J.F. *Etude théorique et numérique de l'évolution morphologique d'interfaces* Ph.D. thesis, Orsay 1994.

[19] I. Stakgold. *Green's functions and boundary value problems*, 1979, A Wiley-Interscience Series of Texts.

[20] Wilders, P. *Minimization of dispersion in difference methods for hyperbolic conservation laws*, Ph.D. thesis, University of Amsterdam (1983)

[21] Wooding, R.A. *Steady state free convection of liquid in a saturated porous medium*, J. Fluid Mech. **2** (1957), p.p. 273-285.

[22] Wooding, R.A. *Free convection of fluid in a vertical tube filled with porous material*, J. Fluid Mech **13** (1962), p.p. 129-144.

[23] Zhang, H. *Nonlinear degenerate diffusion problems*, PhD thesis, Delft University of Technology, The Netherlands.